Radiolabeled Polymeric Nanoconstructs Loaded with Docetaxel and Curcumin for Cancer Combinatorial Therapy and Nuclear Imaging

*Cinzia Stigliano, Jaehong Key, Maricela Ramirez, Santosh Aryal, and Paolo Decuzzi**

Growing evidence suggests that multifaceted diseases as cancer can be effectively tackled by hitting simultaneously different biological targets and monitoring patient-specific responses. Combinatorial therapies, relying on the administration of two or more molecules with different cytotoxic mechanisms, are rapidly progressing in the clinic. Here, 100 nm spherical polymeric nanoconstructs (SPNs) are proposed for the combinatorial treatment of tumors by codelivering a potent antimitotic drug—docetaxel (DTXL)—and a broad spectrum anti-inflammatory molecule—curcumin (CURC). In vitro, SPNs loaded with DTXL and CURC induce a threefold decrease in IC_{50} as compared to DTXL-loaded SPNs. This synergic antitumor effect is also significant in mouse models of glioblastoma multiforme, where, after 22 d of treatment, the combinatorial approach leads to complete disease regression. At 90 d post-treatment initiation, mice injected with DTXL + CURC SPNs have a 100% survival, whereas only 50% of the DTXL SPN treated mice survive. SPNs are also labeled with radioactive ^{64}Cu(DOTA) molecules to document, via PET imaging, the progressive tumor mass shrinkage. Sensitization of DTXL by CURC is associated with NF-κB downregulation and increased apoptosis. These theranostic nanoconstructs could be used for combinatorial treatment and assessment of therapeutic efficacy in other malignancies.

1. Introduction

The past decade has witnessed an impetuous development of nanoconstructs for the systemic and controlled delivery of therapeutic and imaging molecules for the early detection, imaging, and treatment of malignancies.[1] Nanoconstructs with different sizes, surface properties, shapes, and material compositions have been demonstrated to successfully modulate the bioavailability of therapeutic molecules, such as doxorubicin, docetaxel, cisplatin, and several others, increasing their tumor accumulation while reducing off-site effects.[2] Perhaps, even more interesting is the fact that nanoconstructs can be engineered to deliver different therapeutic agents to a malignant mass simultaneously impacting multiple subcellular targets. In this respect, growing evidence suggests that combinatorial therapies,[3] where conventional antitumor drugs are administered together with molecularly targeted agents, are more promising than traditional "one-size-fits-all" therapeutic approaches.[4] By simultaneously loading and delivering different molecules into nanoconstructs, the benefits of combinatorial therapies could be enhanced even more. Furthermore, nanoconstructs can carry imaging agents, for instance radioisotopes for positron emission tomography (PET) imaging, gadolinium compounds, or iron oxide nanoparticles for magnetic resonance imaging (MRI).[5] As such, nanoconstructs can be employed for treating a malignant mass and simultaneously assessing the efficacy of the intervention over time, in a patient-specific manner.[6]

In combinatorial therapies, often an antitumor drug is associated with a sensitizing agent that could boost the cytotoxic effect of the former alleviating drug resistance and disease recurrence. Among all chemotherapeutic drugs available in the clinic, docetaxel (DTXL) is one of the most potent but is also characterized by significant adverse effects. In order to modulate off-site cytotoxicity, the maximum injectable dose of DTXL is limited that, on the other hand, tends to favor the selection of refractory cancer cell clones and occurrence of drug resistance.[7] This has been especially reported in aggressive cancers that tend to evade chemotherapy by modulating regulatory pathways of cell survival and apoptosis. Specifically, it has been documented that DTXL, as well as other anticancer drugs, can upregulate two fundamental pathways for cell survival: PI3K/AKT and nuclear factor-κB (NF-κB).[8] The inhibition of either one or both molecules could sensitize cancer cells to DTXL,

Dr. C. Stigliano, Dr. J. Key, M. Ramirez, Dr. S. Aryal, Dr. P. Decuzzi
Department of Translational Imaging
Houston Methodist Research Institute
Houston, TX 77030, USA
E-mail: pdecuzzi@houstonmethodist.org; paolo.decuzzi@iit.it

Dr. J. Key
Department of Biomedical Engineering
Yonsei University
Gangwon 220-710, Korea

Dr. S. Aryal
Nanotechnology Innovation Center of Kansas State (NICKS)
Kansas State University
Manhattan, KN 66506, USA

Prof. P. Decuzzi
Department of Drug Design and Development
Fondazione Istituto Italiano di Tecnologia
Genova 16163, Italy

DOI: 10.1002/adfm.201500627

increasing antitumor efficacy and reducing resistance.[9] In this context, a potential chemo-sensitizer for DTXL could be curcumin (CURC), a natural compound from curcuma longa, which offers a very broad spectrum of action and quite interesting therapeutic effects.[10] CURC is an anti-inflammatory molecule that inhibits the AKT pathway and downregulates cyclooxygenase-2 (COX-2),[11] but it is also effective in downregulating NF-κB, a key transcription factor in tumorigenesis, angiogenesis,[12] and apoptosis.[13] Interestingly, NF-κB is constitutively active or overexpressed in several human carcinomas.[14] In these malignancies, CURC could efficiently synergize with DTXL by blocking the NF-κB transcription factor.

The goal of this paper was to investigate the in vivo potential of multifunctional nanoconstructs capable of delivering multiple therapeutic and imaging agents for cancer combinatorial therapy and for assessing the outcome of the intervention via imaging. The proposed nanoconstructs consist of a hydrophobic poly(lactic-*co*-glycolic acid) (PLGA) polymeric core stabilized by an external monolayer of phospholipids and poly(ethylene glycol) (PEG) chains. The hydrophobic core contains two therapeutic molecules, docetaxel (DTXL) and curcumin (CURC), whereas radioactive molecules ^{64}Cu(DOTA) are directly conjugated to the phospholipid monolayer for PET imaging. The nanoconstructs are spherical in shape with a characteristic diameter of about 100 nm, which is ideal for targeting solid tumors via the enhanced permeability and retention (EPR) effect. After the physico-chemical and in vitro biological characterizations, these multifunctional spherical polymeric nanoconstructs (SPNs) are tested in vivo for their therapeutic and imaging efficacy in mice bearing U-87 MG tumor cells.

2. Results and Discussion

2.1. Synthesis and In Vitro Characterization of Multifunctional Spherical Polymeric Nanoconstructs (SPNs)

Polymeric nanoconstructs were synthetized via a nanoprecipitation method, following a standardized protocol already described by the authors.[5a,b] As shown in **Figure 1**A, SPNs consist of a polymeric core of PLGA, physically entrapping hydrophobic therapeutic molecules—docetaxel (DTXL) and curcumin (CURC)—and a surface phospholipid monolayer, including Egg PG and pegylated DSPE-PEG-COOH, stabilizing the whole system. 1,4,7,10-Tetraazacyclododecane-1,4,7,10-tetraacetic acid (DOTA) molecules can be directly conjugated to the phospholipid monolayer and then reacted with copper salts to obtain ^{64}Cu(DOTA) radiolabeled nanoconstructs. In the present study, two different types of SPNs were synthetized: i) SPNs loaded with docetaxel alone (DTXL SPNs) and ii) SPNs coloaded with docetaxel and curcumin (DTXL + CURC SPNs). Dynamic light scattering (DLS) analysis shows a monodisperse population of SPNs with a hydrodynamic diameter of about 90 nm and a low polydispersity index (PDI < 0.150), for both formulations (Figure 1B and **Table 1**). No lipid aggregates and micelles were detected by DLS also after 1 week in buffer saline pH 7.4 (data not shown).[5a] The surface electrostatic charge was of about –60 mV, likely associated with the carboxylate groups of the DSPE-PEG-COOH (Table 1). Note that the hydrodynamic size (≈100 nm) and surface properties (charge and pegylation) of SPNs are ideal for their passive and progressive accumulation within the tumor mass via the enhanced permeability and retention effect (EPR).[15] As shown by scanning electron microscopy images (Figure 1C and Figure S1, Supporting Information), nanoconstructs exhibit a regular, spherical shape and a quite homogeneous size that is not significantly affected by the two different loading conditions. Additional details on the structure of SPNs are provided by the transmission electron microscopy (TEM) image of Figure 1D. Specifically, a uranyl acetate staining has been performed to enhance the electron contrast between the superficial lipid monolayer (dark ring) and the polymeric core (bright core) (Figure 1D and inset).

The therapeutic molecules DTXL and CURC were coloaded within the SPN hydrophobic core and standard liquid chromatography was used to quantify loading amounts and release profiles. As listed in **Table 2**, 1 mg of DTXL + CURC SPNs contains almost equal amounts of the two molecules, namely 23.35 μg of DTXL and 27.55 μg of CURC, resulting in encapsulation efficiencies of 32.445% and 76.547%, respectively. On the other hand, 1 mg of DTXL SPNs contains 30.81 μg of DTXL, resulting in an encapsulation efficiency of 40.83% (Table 2).

To complete the in vitro physical–chemical characterization of SPNs, release studies have been also performed in PBS, at pH 7.4 and 37 °C, up to 72 h postincubation for both loading conditions. **Figure 2**A,B shows the experimental release curves for DTXL + CURC SPNs and DTXL SPNs, respectively. Notably, the release kinetics of DTXL, either alone or in the presence of CURC, are comparable demonstrating both the reproducibility of DTXL release and the lack of interference with CURC. Note that this was already observed for the loading and encapsulation efficiency. Specifically, 20%, 30%, and 40% of DTXL are released within the first 2, 6, and 24 h. At 72 h, almost 90% of the loaded DTXL is released. This long-term release of DTXL is most likely controlled by the surface lipid monolayer and the progressive degradation of the PLGA matrix.[17] The release of CURC is faster than DTXL with almost 80% of CURC being released already at 24 h. The release kinetics of DTXL and CURC have been interpreted within the Ritger–Peppas model (Supporting Information). For all three configurations (DTXL alone, DTXL, and CURC), a biphasic release profile has been observed with almost 80% of the total drug mass released within the first 48 h by pure Fickian diffusion (n = 0.5 in the Ritger–Peppas model). This is in agreement with other studies on the release kinetics of hydrophobic molecules from PLGA-based systems.[16] Note also that CURC is released at higher rates (k = 13.443 [$h^{-1/2}$]) than DTXL ($k \approx 11.2$ [$h^{-1/2}$]). This should be mostly attributed to the lower size of CURC (MW 368.38) as compared to DTXL (MW 807.88) and higher aqueous solubility of CURC (≈0.6 μg mL^{-1}) as compared to DTXL (≈0.3 μg mL^{-1}). Moreover, the presence of CURC in SPNs does not significantly affect the release of DTXL: during the first phase, k = 11.248 and 11.177 [$h^{-1/2}$] in the absence and presence of CURC, respectively, with only 0.6% difference. Note that during the second phase, the mass of DTXL released is minimal.

The in vitro cell killing efficacy of SPNs was assessed on a glioblastoma multiforme cell line (U-87 MG). Cells were

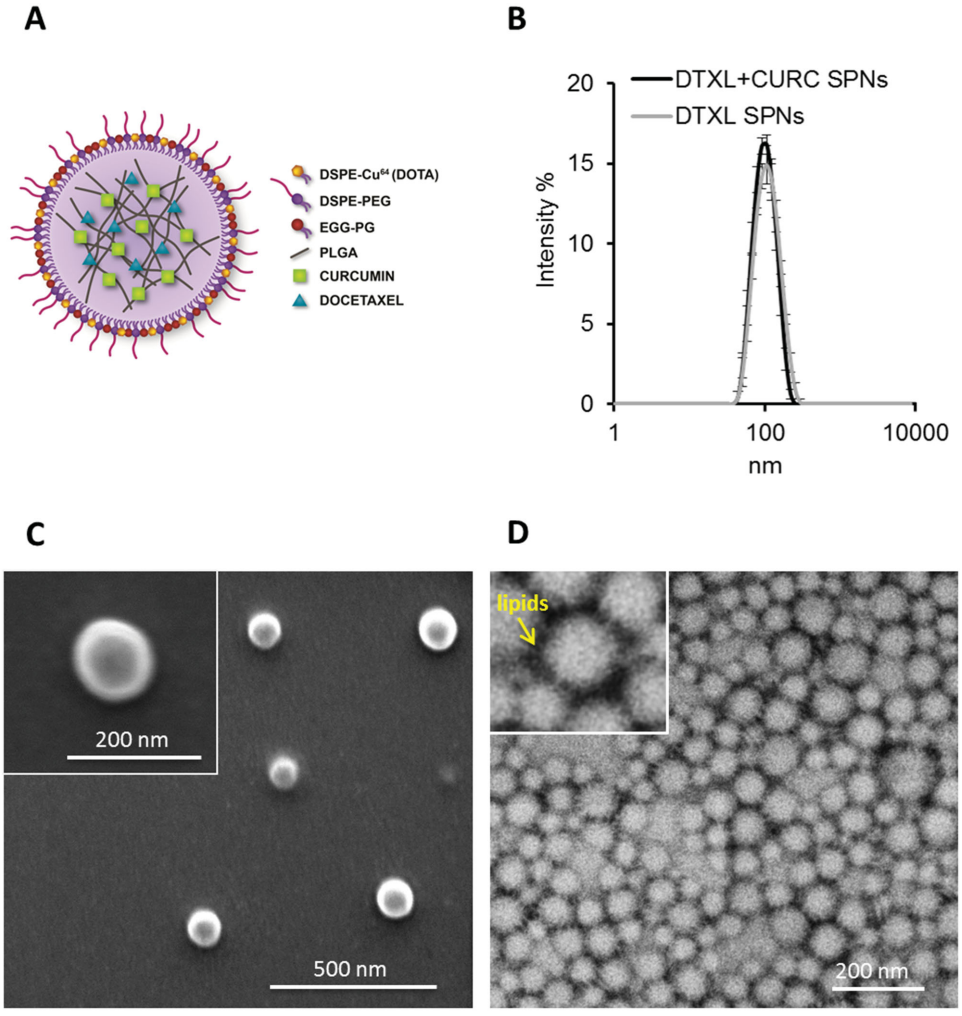

Figure 1. Spherical polymeric nanoconstructs (SPNs): phyisco-chemical characterization. A) Schematic illustration of SPNs synthetized via nanoprecipitation comprising a poly(lactic-*co*-glycolic acid) (PLGA) core loaded with therapeutic molecules and stabilized by an external lipid monolayer (DSPE-PEG and Egg-PG or DSPE-^{64}Cu (DOTA)). B) Size distribution of SPNs by DLS analysis. Data are mean ± SD ($n = 3$ samples measured ten times each). C) Scanning electron microscopy (SEM) image of SPNs loaded with docetaxel and curcumin. D) Transmission electron microscopy (TEM) image of SPNs after uranyl acetate staining to enhance the electron contrast between the superficial lipid monolayer (dark ring) and the polymeric core (bright core). Inset shows the darker uniform layer of lipids surrounding the polymeric core.

incubated with different concentrations of DTXL + CURC SPNs and DTXL SPNs in order to estimate the IC_{50} values at 72 h. Figure 2C shows the percentage of viable cells as a function of SPN concentrations. The same data are rescaled in terms of DTXL amounts loaded into SPNs and presented in Figure S3 (Supporting Information). The treatment of U-87 MG cells with DTXL SPNs resulted in an IC_{50} of 5.09 μg mL^{-1} of nanoconstructs (34 × 10^{-9} M of DTXL). More interestingly, the coloading of CURC significantly enhances the cell-killing capability of SPNs reducing even more the IC_{50} to 1.23 μg mL^{-1} of nanoconstructs (12 × 10^{-9} M of DTXL). This corresponds to a fourfold decrease in SPN concentration and almost threefold reduction in DTXL concentration to achieve the same cell killing effect.

Table 1. Main physical–chemical parameters of SPNs.

	DTXL + CURC SPNs	DTXL SPNs
Diameter [nm ± s.d.]	89.58 ± 2.32	98.16 ± 1.87
PdI	0.141	0.145
Zeta potential [mV]	−65.0 ± 3.5	−63.7 ± 2.4

Table 2. Drug loading amounts, loading, and encapsulation efficiencies for SPNs.

	DTXL + CURC SPNs		DTXL SPNs
	DTXL	CURC	DTXL
μg Drug/mg SPNs	23.348 ± 0.441	27.552 ± 1.54	30.813 ± 1.21
L.E.%	2.334	2.755	3.081
E.E.%	32.445	76.547	40.828

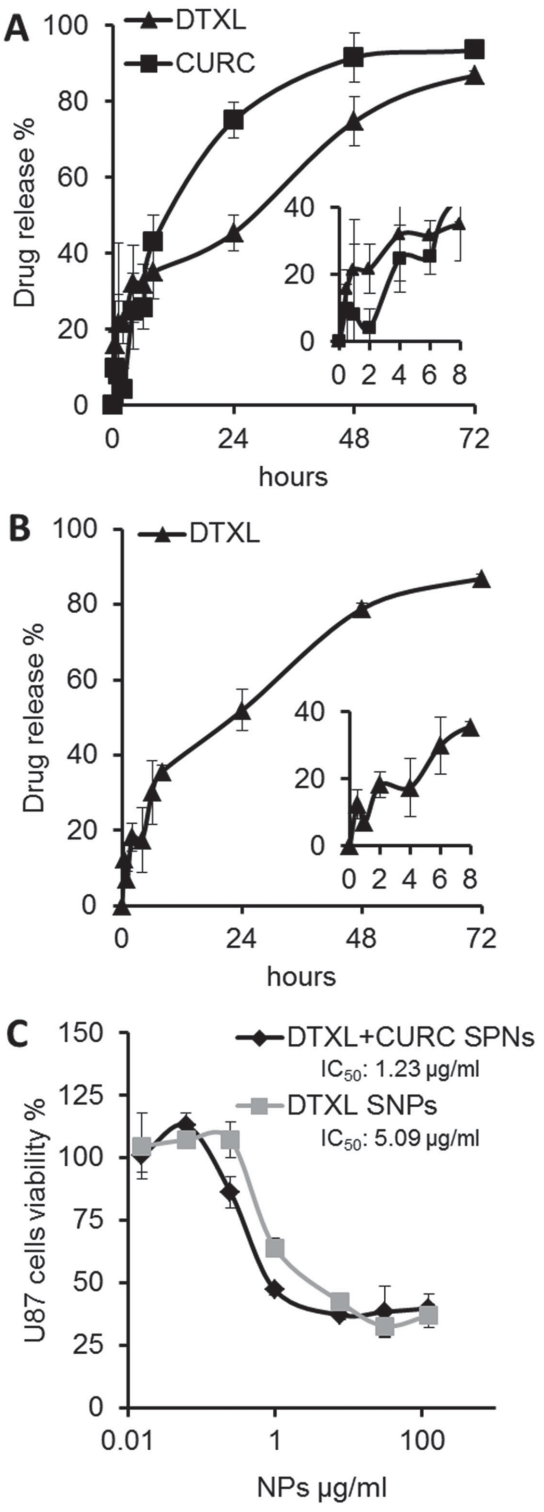

Figure 2. Spherical polymeric nanoconstructs (SPNs): drug loading and release, cytotoxicity. Release profiles of SPNs loaded A) with the combination of docetaxel (DTXL) and curcumin (CURC) and B) with only DTXL (in PBS, at 37 °C). C) In vitro cell viability at 72 h for U-87 MG cells incubated with SPNs loaded with docetaxel and curcumin (DTXL + CURC SPNs), and with DTXL alone (DTXL SPNs). IC_{50} values are expressed as µg mL^{-1} of SPNs.

2.2. In Vivo Efficacy of SPNs in Glioblastoma Multiforme Tumor Bearing Mice

To determine the efficacy of DTXL and DTXL + CURC loaded nanoconstructs on tumor growth, SPNs containing 80 µg of DTXL (≈4 mg kg^{-1}) were systemically injected into mice bearing a nonorthotopic glioma. Specifically, U-87 MG cells were injected into the flank of a mouse and allowed to grow for about 2 weeks. As control experiments, saline solution, and 80 µg of clinical grade, commercially available DTXL (free DTXL) were used. SPNs were injected every 2 d up to 22 d, for a total number of injections equal to 12. Note that the injected dose of DTXL (≈4 mg kg^{-1}) is significantly smaller than the doses conventionally used in these experiments, which ranges between 10 and 20 mg kg^{-1} of DTXL per animal mass. In **Figure 3**A–C, tumor growth curves are plotted up to 40 d for the four different treatment groups, namely DTXL SPNs, DTXL + CURC SPNs, free DTXL, and saline.

The tumor mass developing in control mice (saline injection) continuously grew over time up to ≈5 cm^3 in 30 d. The mice treated with systemically injected free DTXL showed an initial response with a significant reduction in tumor mass within the first 2 weeks, which was then followed by a progressive growth demonstrating relapsing of the malignant mass (Figure 3B). The behavior of the growth curves for tumors treated with SPNs was very different. For both DTXL SPNs and DTXL + CURC SPNs, the tumor mass started reducing already after 1 week. For SPNs loaded with DTXL and CURC complete regression of the malignant mass was observed at 32 d post-treatment initiation, whereas it took about 1 more week (38 d) to reach a similar result with DTXL SPNs. The rate of tumor shrinkage was faster for the mice treated with the combination rather than with DTXL alone, thus demonstrating also in vivo the synergy between DTXL and CURC. Most importantly, some of the mice treated with DTXL SPNs showed recurrence of the disease after a few weeks, as documented by the tumor volume data of Figure 3C and the Kaplan–Meier curves of Figure 3D. Specifically, at 90 d, 50% of mice treated with DTXL SPNs were sacrificed for excessive tumor size (about 5 cm^3), whereas a 100% survival was documented for mice treated with DTXL + CURC SPNs at the same time point. As a control, the percent survival of mice treated with saline dropped to 50% and 100% at 23 and 33 d post-treatment initiation, respectively. The mouse weight was monitored throughout the experiment to assess any severe toxicity related to the treatment. For all groups, a moderate reduction in mouse weight was observed over the first 22 d of treatment. As the treatment was completed, all mice progressively regained the lost weight and at 40 d no difference was observed as compared to the initial conditions (Figure S4, Supporting Information). This moderate loss of weight should be attributed to the well-known toxicity of DTXL, which can cause reduction in the white blood cell count (neutropenia), as experienced also in patients as a common side effect of taxols.[7] Overall, treatments with SPNs were well tolerated by mice without resulting in hypersensitivity or anaphylactic reactions. Note that the present data demonstrate a complete tumor regression at DTXL doses far lower than the conventionally injected doses (≈4 vs 10–20 mg kg^{-1} of DTXL per animal mass).

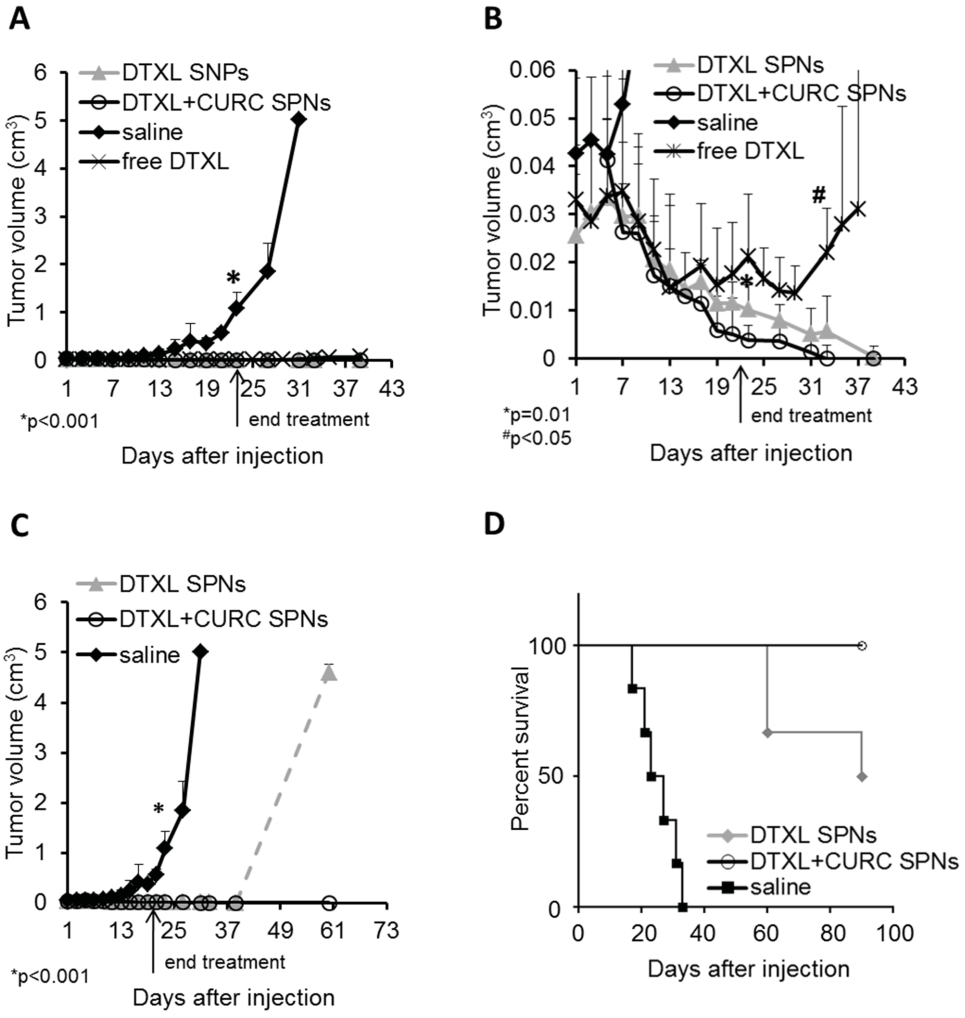

Figure 3. In vivo therapeutic studies with SPNs. Experiments were performed in mice bearing glioblastoma multiforme tumors by systemic injection of: free DTXL; saline solution; DTXL SPNs; and DTXL+CURC SPNs. A–C) Tumor growth curves comparing the efficacy of the four different experimental groups. Data are mean tumor volumes ± SD ($n = 6$ per treatment group). *$p < 0.001$ is for DTXL + CURC SPNs versus saline, and DTXL SPNs versus saline at the end of the treatment. *$p = 0.01$ is for DTXL + CURC SPNs versus DTXL SPNs at the end of the treatment. #$p < 0.05$ is for DTXL + CURC SPNs versus free DTXL at day 33. *$p < 0.001$ is for DTXL + CURC SPNs versus saline, and DTXL SPNs versus saline at the end of the treatment. D) Kaplan–Meier curves of survival.

2.3. PET Imaging for Monitoring Tumor Progression and Response to Therapy

SPNs were labeled with ^{64}Cu in order to assess their biodistribution and tumor accumulation during treatment. Radioactive copper was chelated via lipid–DOTA molecules distributed over the SPN lipid monolayer (Figure 1A). PET/CT imaging of the whole animal was performed at 24 h postinjection. **Figure 4**A shows representative images of the distribution of ^{64}Cu-SPNs in mice at the time zero and 2 weeks after treatment initiation with DTXL + CURC SPNs. High activity is detected mostly in the abdominal cavity, including the liver, bladder, and intestine, suggesting hepatic metabolization of SPNs and excretion of ^{64}Cu through both the hepato-biliary circulation and kidneys. However, most importantly, a strong tumor signal was detected at time zero, mediated by the progressive accumulation of SPNs via the EPR effect.[5b] At 2 week post-treatment initiation, the tumor-associated activity was much lower (Figure 4A). The SPNs accumulation in tumor was of ≈4% the injection dose per gram of tumor (% ID g^{-1}) at time zero and reduced to ≈2% after 2 weeks of treatment (Figure 4B). A CT analysis of the tumor volume also documented the shrinkage of the malignant mass from 50 to 30 mm^3 over the same period. The lower uptake of circulating nanoconstructs should be associated with the actual response of the tumor mass to the SPN-mediated therapy, which induces cell apoptosis and tumor shrinkage.

2.4. Apoptosis and Expression of NF-κB in Tumor Tissues

In order to better characterize the contribution of CURC to tumor mass decrease, at 2 week post-treatment initiation, the density of apoptotic tumor cells within the malignant tissue was assessed via TdT-mediated dUTP nick end labeling assay

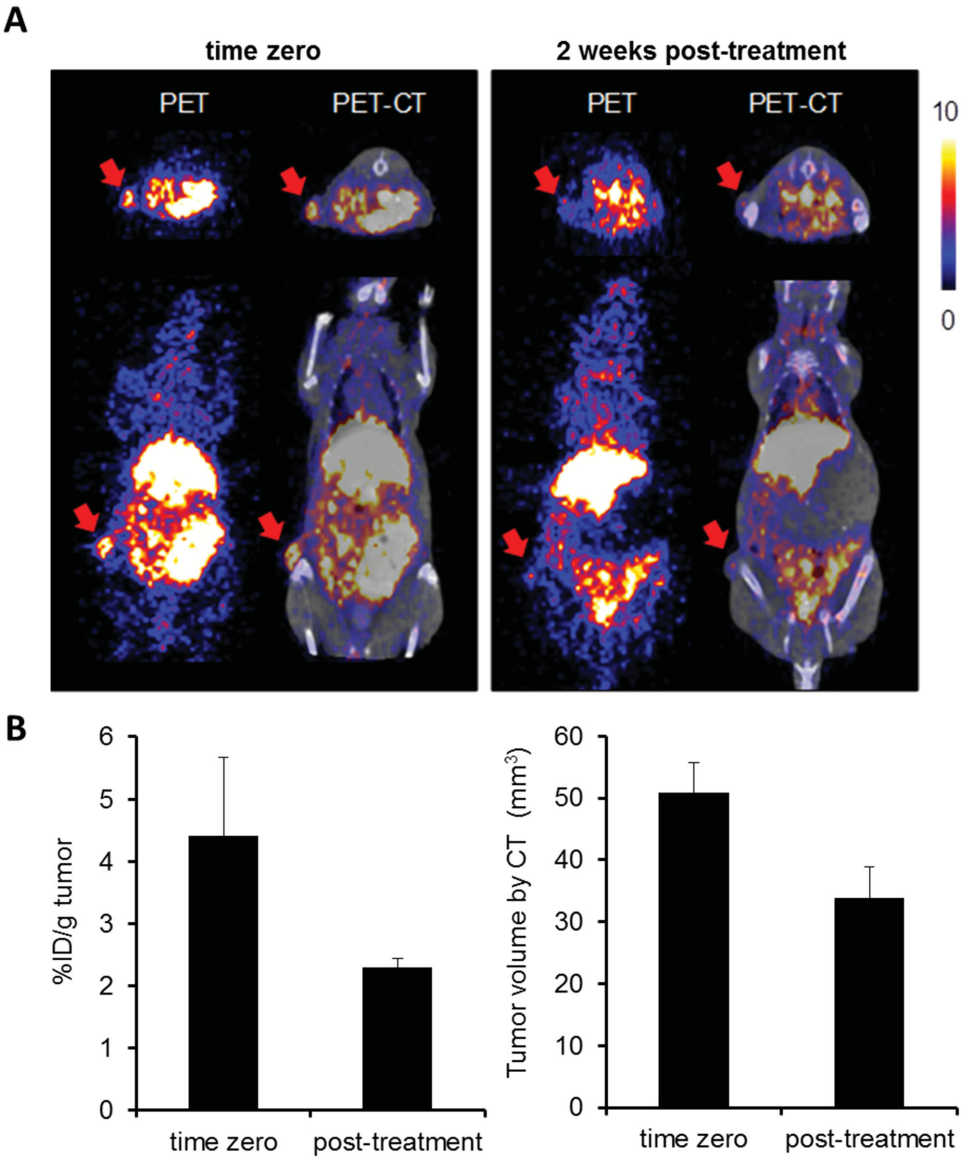

Figure 4. PET/CT imaging with ^{64}Cu(DOTA) radiolabeled SPNs. A) In vivo distribution of ^{64}Cu(DOTA)-SPNs before (time zero) and 2 week after treatment initiation with DTXL + CURC SPNs. Transverse (top) and coronal (bottom) planes are shown. Red arrows indicate SPNs accumulation in tumors. B) Quantification of ^{64}Cu(DOTA)-SPN accumulation in tumors expressed as percent of injected dose per gram of tissue (left) and tumor volume measurement via CT (right).

(TUNNEL assay). **Figure 5**A shows the apoptotic index, defined as number of stained apoptotic cells per section, derived from representative histological slides of the tumor tissue. These data confirm a fourfold increase in apoptosis for tumors treated with DTXL + CURC SPNs as compared to DTXL SPNs. Since the chemio-sensitizing effect of CURC has been suggested to be associated with down regulation of NF-κB,[8b,10] Figure 5B shows the density of this molecule in representative histological slides of tumor tissue. In the saline-treated tumors, the NF-κB staining was intense and widespread all over the section. The signal was slightly lower in intensity for mice treated with DTXL SPNs. Finally, in tumors treated with DTXL + CURC SPNs, a significant suppression of NF-κB signal was observed. The staining was remarkably reduced and several cells were not even marked. Also, the presence of some apoptotic cells characterized by cytoplasmic shrinkage and nuclear chromatin condensation is obvious. The expression of the transcription factor NF-κB (p65) was estimated also via Western blotting at the same time point for tumors treated with DTXL + CURC SPNs, DTXL SPNs, and saline (Figure 5C). The densitometry analysis of the bands showed a significant approximately twofold reduction of the NF-κB (p65) expression in tumors treated with DTXL + CURC SPNs as compared to the saline control (Figure S5, Supporting Information). It is assumed that the high apoptosis level and the regression of the tumor volume were signs of degeneration of the tissue due to the combined treatment, which was sufficient

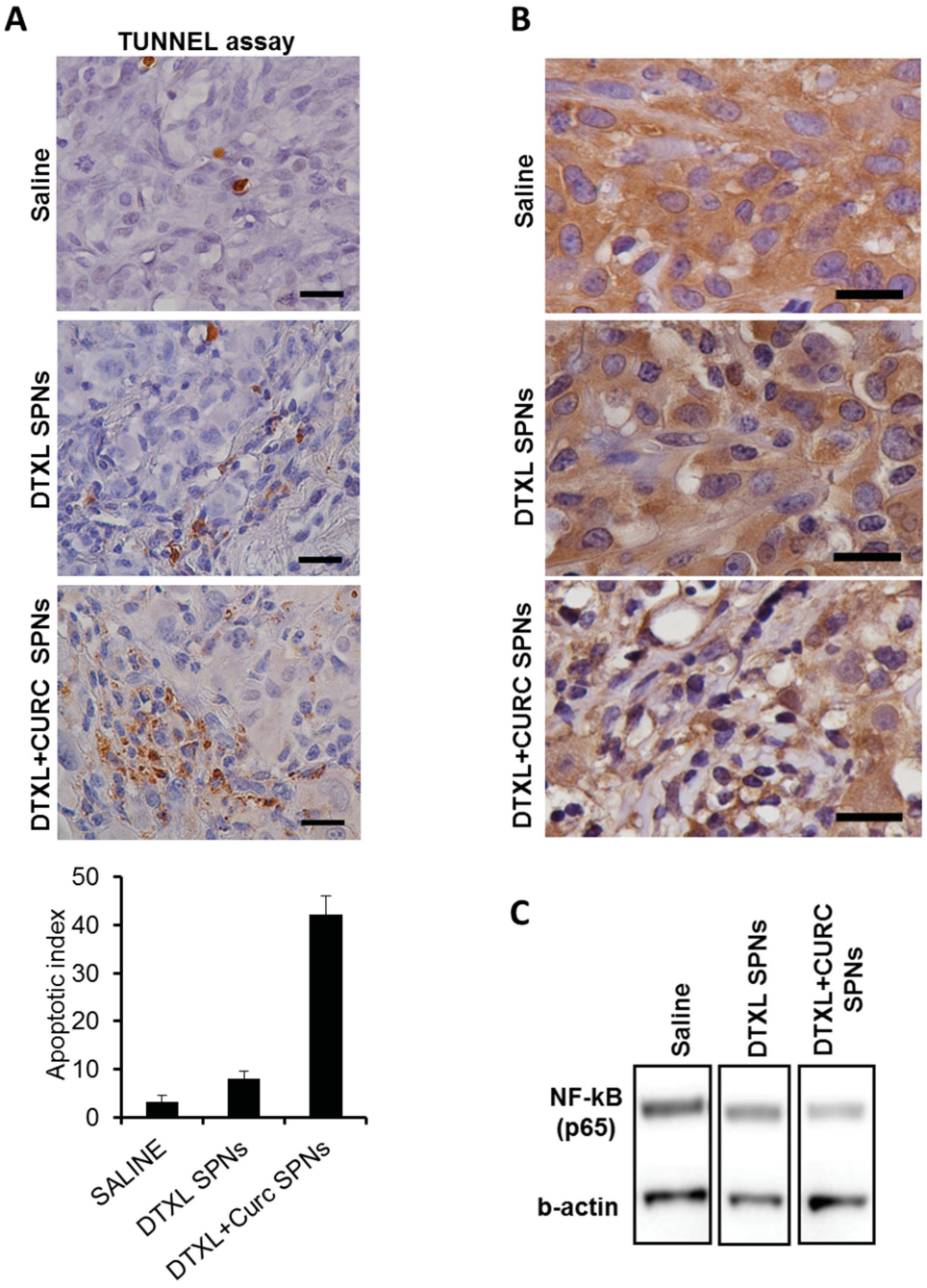

Figure 5. Histological analysis of tumor tissue. A) Quantification of the apoptotic index in tumors at 2 week post-treatment with saline, DTXL SPNs, and DTXL + CURC SPNs, using a TUNNEL assay. B) NF-κB (p65) immunohistochemistry sections from tumors at 2 week post-treatment with saline, DTXL SPNs, and DTXL + CURC SPNs. C) NF-κB (p65) protein quantification by Western blotting in tumors at 2 week post-treatment.

to cause a suppression of NF-κB. Moreover, the CURC effect is expected to be higher and more significant after a longer treatment, but the complete regression of tumor masses after 22 d did not allow for a careful molecular analysis post-treatment completion. This again confirms that CURC has the expected effect on tumor cells and contributes synergistically with DTXL. Note that the amount of CURC used in this study was much lower than conventional doses employed to induce antitumor effect.[10]

3. Conclusions

In this paper, theranostic nanoconstructs were presented for the combinatorial treatment of tumors, with a potent chemotherapic molecule—docetaxel (DTXL)—and a broad-spectrum natural anti-inflammatory compound—curcumin (CURC), and for simultaneously monitoring the response to therapy via PET/CT imaging. It was shown that the cotreatment with DTXL and

CURC, which were loaded and delivered with the same nanoconstruct, led to complete malignancy regression within 32 d post-treatment initiation with no observed recurrence up to 90 d. It was also demonstrated that CURC down-regulates the expression of the transcription factor NF-κB that, as discussed by other authors, could be responsible for sensitizing the therapeutic effect of DTXL. This would explain the improved efficacy of the proposed combinatorial therapy (DTXL + CURC SPNs) as compared to conventional delivery of the sole chemotherapic molecule DTXL. A twofold decrease in the accumulation of nanoconstructs within the malignant mass was detected during the treatment demonstrating that SPNs can be simultaneously used for cancer treatment as well as for assessing therapeutic response. The proposed theranostic nanoconstructs could be beneficial in the treatment also of other malignancies.

4. Experimental Section

Materials: 1,2-Distearoyl-*sn*-glycero-3-phosphoethanolamine-*N*-[succinyl(polyethylene glycol)-2000] (DSPE-PEG-COOH) and L-α-phosphatidyl-DL-glycerol (Egg PG, Chicken) were purchased from Avanti Polar Lipid Inc. *N*-Hydroxysuccimidyl ester activated 1,4,7,10-tetraazacyclododecane-1,4,7,10-tetraacetic acid (DOTA-NHS) was purchased from Macrocyclics, Inc. Poly(D,L-lactide-*co*-glycolide) acid terminated (50:50), mw 38 000-54, was purchased from Sigma-Aldrich, curcumin 98+% was purchased from Acros Organics, and docetaxel was purchased from ChemieTek. Clinical grade docetaxel was purchased from Sagent Pharmaceuticals. All other chemicals and solvents were purchased from Sigma-Aldrich.

Synthesis and Characterization of SPNs: SPNs were synthetized by nanoprecipitation method. Briefly, Egg PG (200 μg) and DSPE-PEG-COOH (260 μg) were dissolved in 4% ethanol at 65 °C. To this solution, PLGA (100 μg) and drugs (100 μg of docetaxel (DTXL) and 50 μg of curcumin (CURC), respectively, used alone or in combination) dissolved in acetonitrile were added dropwise while heating and stirring. Then, water (1 mL) was added to reduce the temperature and the mixture was stirred at room temperature for 2 h for the solvent evaporation. Finally, the SPNs were washed with water by centrifugation using Amicon Ultra-4, Centrifugal Filter 10 000 Da (Millipore) at 3500 rpm for 8 min for three times. For the radiolabeling with ^{64}Cu, the SPNs were synthetized following the same procedure previously described with the substitution of the Egg PG with lipid-DOTA (200 μg) (the synthesis of lipid-DOTA is described below); after purification the SPNs were resuspended in acetate buffer (pH 5.5) and incubated with 100 μCi 64Cu for 1 h. The SPNs size and surface zeta potential were estimated by dynamic light scattering (DLS) (Malvern Zetasizer, ZEN 3600). The Smoluchowski model was used to calculate the zeta potential values. All data represent ten measurements from each sample resuspended in deionized water. Scanning electron microscopy (SEM) was conducted by using FEI Nova NanoSEM 230; the SPNs were dropped directly onto a polished silicon wafer and after drying sputter-coated with platinum prior to imaging. The samples for transmission electron microscopy (TEM) were prepared by the drop casting method over copper grid. The sample were negatively stained for 10 min with 2% (w/v) uranyl acetate aqueous solution, and then washed twice with distilled water and dried before imaging.

Synthesis of Lipid-DOTA: The lipid-DOTA was synthetized as described in our previous publications with slight modification.[5b] Briefly, DSPE (100 mg, 0.13 mmol) was dissolved in chloroform:methanol. To this solution, DOTA-NHS (100.3 mg, 0.2 mmol) dissolved in water was added resulting in the final ratio of solvent mixture of 1.0:0.5:0.007 (chloroform:methanol:water). The reaction was carried out for 6 h in the presence of a catalytic amount of triethylamine (TEA). Then, the product was precipitated in cold diethyl ether and further purified by the repeated precipitation method.

Drug Loading and Release Study: To measure the loading of DTXL and CURC, and the release profile, nanoparticles were suspended in phosphate buffer (pH 7.4) to obtain 1 mg mL^{-1} solution concentration. The solution was fractioned in disposable dialysis cups (Slide-A-Lyzer MINI Dialysis Units, 10 000 MWCO, Thermo Scientific), in triplicate for each time point. These cups were dialyzed in 4 L of PBS pH 7.4 at 37 °C with gentle stirring. Every 24 h the PBS was chanced with fresh one. At each time point, the SPNs solution was collected from the cups and mixed with an equal volume of acetonitrile to dissolve the SPNs. The amount of residual drugs in the SPNs was estimated by HPLC (Agilent Thechnologues 1200 Infinity series) using a column Luna 5u C18(2) 100A, 250 × 4.6 mm (Phenomenex). DTXL and CURC absorbance was measured by UV–vis detector at 227 and 430 nm with 1 mL min^{-1} flow, 50:50 acetonitrile:water mobile phase.

Cell Viability Measurement: U-87 MG cells from ATCC were maintained in EMEM medium from Corning, supplemented with 10% FBS and 1% penicillin/streptomycin (Invitrogen). Cell were incubated at 37 °C in 5% CO2 atmosphere. Cell viability was determined using the TACS XTT kit (Trevigen) after 72 h of incubation with SPNs loaded with drugs. Cell were plated in 96-well plates at 10 000 cells per well concentration and cultured for 24 h. DTXL SPNs and DTXL + CURC SPNs were resuspended in complete medium at different concentrations and used to culture the cells. The XTT working solution was added according to the manufacturer's instructions. The absorbance was measured at 490 nm in a microplate reader (SynergyH4, Bioteck), and the data were collected when the absorbance was between 0.8 and 1.2. Cell viability was normalized to that of untreated cells.

Animals: Female athymic nude mice 7–8 weeks old were purchased from Charles River. All studies were approved by The Methodist Hospital Research Institute Institutional Animal Care and Use Committee.

Tumor Model and Therapy Experiments: For the U-87 MG xenograft tumor model, 3 × 10^6 cells were resuspended in PBS (100 μL) and subcutaneously injected at the lower flank of the mouse. 8–10 d after the cells injection, the mice were randomized into four groups (six mice per group). The groups were dosed for 23 d by retro-orbital injection every 2 d with DTXL + CURC SPNs, DTXL SPNs, free DTXL, and saline, respectively. Each injected dose contained 80 μg of docetaxel into SPNs or as commercial clinical formulation. Therapy experiment was done after 23 d commencing therapy. During the treatment period, the mice were sacrificed when the tumor size was approximately 2 cm in diameter. Tumor growth was calculated by tumor volume (V) with the formula $V = W^2 \times L/2$ (W = width; L = length). The survivor mice were observed up to 90 d. To determine the effect of the SPNs treatment on tumor markers, three groups of mice were treated with the same dosing for 1 week with DTXL + CURC SPNs, DTXL SPNs, and saline. Tumors were harvested and processed for protein extraction and histology.

PET/CT Imaging: Nude mice (n = 2) with U-87 MG subcutaneous tumor were used for PET/CT imaging. The PET/CT scan was performed after intravenously injections with ^{64}Cu SPNs (≈40 μCi) at the begging of the treatment and after 2 weeks of treatment (seven injections in total) with DTXL + CURC SPNs and saline at same dosage of the therapy study. The scanner is a murine-dedicated multimodal PET/SPECT/CT system (Siemens, Inveon). The mice were imaged using medium resolution CT parameters for 5 min and immediately followed by PET acquisition for 20 min, at 24 h postinjection of ^{64}Cu-SPNs. CT image reconstruction was obtained with the default common cone-bean reconstruction algorithm of the scanner (COBRA). PET images were reconstructed by the 2D ordered subset expectation maximization algorithm (OSEM2D). No correction was applied for PET attenuation or scatter. PET and CT images were coregistered and viewed using the Inveon Research Workplace software (Siemens).

Immunohistochemistry: The tumors were collected after 1 week of treatment, formalin-fixed and paraffin-embedded. IHC was performed for NF-κB (p65) by Research Pathology Core Lab of The Houston Methodist Research Institute. Images were taken with NIKON eclipse 80i inverted microscope and using camera Nikon digital sight DS-U3 and NIS-Element software. To quantify apoptosis TUNNEL assay was performed and apoptotic index was determined by the number of apoptotic tumor cells in six representative photographs randomly (40× magnification) of each slide.

Western Blot Analysis: Total protein was extracted from the tumor tissues to evaluate the expression of NF-κB (p65) protein. Actin protein expression was used as control for normalization. Briefly, the tissues were washed twice with cold PBS and lysate with RIPA buffer (Thermo Scientific) supplemented with the proteases inhibitor cocktail (Thermo Scientific) for 30 min in ice. The extracted proteins were collected after centrifugation at 21 000 ×*g*, and quantified by BCA assay (Thermo Scientific). The lysates were then analyzed by electrophoresis on 4%–12% (w/v) sodium dodecyl sulfate polyacrylamide gel electrophoresis (SDS-PAGE) gels (Invitrogen). Blotting was performed using a semidry system (Invitrogen). Blots were incubated overnight at 4 °C with primary antibodies diluted 1:500, and then with HRP-conjugated secondary antibodies diluted 1:10 000 for 1 h at RT. All the antibodies were purchased from Santa Cruz. Signals were detected via enhanced chemiluminescence ECL kit (Thermo Scientific) with Li-COR instrument (Bioscience, Lincoln, NE).

Supporting Information

Supporting Information is available from the Wiley Online Library or from the author.

Acknowledgements

The authors acknowledge support from the Translational Imaging Department at the Houston Methodist Research Institute in Houston, TX, USA, via the "TI Pilot Project" initiative; Matthew Landry for the graphic illustration; Nasim Taheri, Arash Bohloul, and Gabriela Escalera for the SEM and TEM imaging.

Received: February 13, 2015
Revised: April 6, 2015
Published online: May 4, 2015

[1] a) A. Wicki, D. Witzigmann, V. Balasubramanian, J. Huwyler, *J. Controlled Release* **2014**, *200*, 138–57; b) D. Peer, J. M. Karp, S. Hong, O. C. Farokhzad, R. Margalit, R. Langer, *Nat. Nanotechnol.* **2007**, *2*, 751; c) M. Ferrari, *Nat. Rev. Cancer* **2005**, *5*, 161; d) V. P. Torchilin, *Adv. Drug Delivery Rev.* **2006**, *58*, 1532.

[2] a) P. Decuzzi, B. Godin, T. Tanaka, S. Y. Lee, C. Chiappini, X. Liu, M. Ferrari, *J. Controlled Release* **2010**, *141*, 320; b) A. L. van de Ven, P. Kim, O. Haley, J. R. Fakhoury, G. Adriani, J. Schmulen, P. Moloney, F. Hussain, M. Ferrari, X. Liu, S. H. Yun, P. Decuzzi, *J. Controlled Release* **2012**, *158*, 148; c) S. Mitragotri, J. Lahann, *Nat. Mater.* **2009**, *8*, 15; d) V. Torchilin, *Eur. J. Pharm. Biopharm.* **2009**, *71*, 431.

[3] a) B. Al-Lazikani, U. Banerji, P. Workman, *Nat. Biotechnol.* **2012**, *30*, 679; b) S. Iadevaia, Y. Lu, F. C. Morales, G. B. Mills, P. T. Ram, *Cancer Res.* **2010**, *70*, 6704.

[4] a) D. J. Slamon, B. Leyland-Jones, S. Shak, H. Fuchs, V. Paton, A. Bajamonde, T. Fleming, W. Eiermann, J. Wolter, M. Pegram, J. Baselga, L. Norton, *N. Engl. J. Med.* **2001**, *344*, 783; b) B. Coiffier, E. Lepage, J. Briere, R. Herbrecht, H. Tilly, R. Bouabdallah, P. Morel, E. Van Den Neste, G. Salles, P. Gaulard, F. Reyes, P. Lederlin, C. Gisselbrecht, *N. Engl. J. Med.* **2002**, *346*, 235.

[5] a) S. Aryal, J. Key, C. Stigliano, J. S. Ananta, M. Zhong, P. Decuzzi, *Biomaterials* **2013**, *34*, 7725; b) S. Aryal, J. Key, C. Stigliano, M. D. Landis, D. Y. Lee, P. Decuzzi, *Small* **2014**, *10*, 2688; c) J. Yuan, H. Zhang, H. Kaur, D. Oupicky, F. Peng, *Mol. Imaging* **2013**, *12*, 203.

[6] a) M. S. Muthu, D. T. Leong, L. Mei, S. S. Feng, *Theranostics* **2014**, *4*, 660; b) S. Ferber, H. Baabur-Cohen, R. Blau, Y. Epshtein, E. Kisin-Finfer, O. Redy, D. Shabat, R. Satchi-Fainaro, *Cancer Lett.* **2014**, *352*, 81; c) J. Xie, S. Lee, X. Chen, *Adv. Drug Delivery Rev.* **2010**, *62*, 1064; d) I. Velikyan, *Theranostics* **2012**, *2*, 424.

[7] J. Baker, J. Ajani, F. Scotte, D. Winther, M. Martin, M. S. Aapro, G. von Minckwitz, *Eur. J. Oncol. Nurs.* **2009**, *13*, 49.

[8] a) W. Chen, X. Wang, L. Bai, X. Liang, J. Zhuang, Y. Lin, *J. Cell Biochem.* **2008**, *105*, 554; b) J. M. Hong, C. S. Park, I. S. Nam-Goong, Y. S. Kim, J. C. Lee, M. W. Han, J. I. Choi, Y. I. Kim, E. S. Kim, *Endocrinol. Metab.* **2014**, *29*, 54.

[9] H. N. He, X. Wang, X. L. Zheng, H. Sun, X. W. Shi, Y. J. Zhong, B. Huang, L. Yang, J. K. Li, L. C. Liao, L. Zhang, L. N. Hu, Y. Lin, *Cancer Lett.* **2010**, *295*, 38.

[10] Y. G. Lin, A. B. Kunnumakkara, A. Nair, W. M. Merritt, L. Y. Han, G. N. Armaiz-Pena, A. A. Kamat, W. A. Spannuth, D. M. Gershenson, S. K. Lutgendorf, B. B. Aggarwal, A. K. Sood, *Clin. Cancer Res.* **2007**, *13*, 3423.

[11] P. Anand, C. Sundaram, S. Jhurani, A. B. Kunnumakkara, B. B. Aggarwal, *Cancer Lett.* **2008**, *267*, 133.

[12] B. B. Aggarwal, *Cancer Cell* **2004**, *6*, 203.

[13] S. Aggarwal, H. Ichikawa, Y. Takada, S. K. Sandur, S. Shishodia, B. B. Aggarwal, *Mol. Pharmacol.* **2006**, *69*, 195.

[14] a) A. Garg, B. B. Aggarwal, *Leukemia* **2002**, *16*, 1053; b) B. B. Aggarwal, B. Sung, *Cancer Discovery* **2011**, *1*, 469.

[15] H. Maeda, *Adv. Enzyme Regul.* **2001**, *41*, 189.

[16] a) J. Siepmann, F. Siepmann, *J. Controlled Release* **2012**, *161*, 351; b) Y. Fu, W. J. Kao, *Expert Opin. Drug Delivery* **2010**, *7*, 429; c) H. K. Makadia, S. J. Siegel, *Polymers* **2011**, *3*, 1377.

[17] J. M. Chan, L. Zhang, K. P. Yuet, G. Liao, J. W. Rhee, R. Langer, O. C. Farokhzad, *Biomaterials* **2009**, *30*, 1627.